



# Skyrmion lattice in a magnetic film with spatially modulated material parameters



M.V. Sapozhnikov <sup>a,b,\*</sup>

<sup>a</sup> Institute for Physics of Microstructures, RAS, Nizhny Novgorod 603950, GSP-105, Russia

<sup>b</sup> N.I. Lobachevskii State University, Nizhny Novgorod 603950, Russia

## ARTICLE INFO

### Article history:

Received 13 May 2015

Received in revised form

3 July 2015

Accepted 25 July 2015

Available online 29 July 2015

### Keywords:

Magnetic skyrmion

Nanomodification

Perpendicular anisotropy

## ABSTRACT

The problem of the skyrmion stability in the magnetic film with perpendicular anisotropy inside the area with the changed material parameters is considered. The solution describing the conditions of such stabilization in the absence of Dzyaloshinskii–Moriya interaction is obtained analytically. The easy method of nanomodification of ordinary magnetic perpendicular media such as Co,Fe/Pt,Pd,Ru superlattices allowing the formation of the dense enough (with the period less than 100 nm) skyrmion lattices is suggested. By micromagnetic simulations it is shown that the skyrmion lattices can be initialized in the system by simple magnetization in the uniform external magnetic field.

© 2015 Published by Elsevier B.V.

## 1. Introduction

Although soliton-like solutions for magnetization distribution carrying topological charge in magnetic materials are well known since the late 1970s [1,2], the new rise of the interest for them is caused by experimental observation of such structures in the chiral magnets [3–5] where they can be stable without the assistance of an external magnetic field [6]. Since these pioneering work such magnetic structures are usually referred to as “magnetic skyrmions”. The special attention to the magnetic skyrmions is caused by their unusual spin–electronic properties, such as the topological Hall effect [7–10], current-driven motion in ultra-low currents [11,12] accompanied by skyrmion Hall effect [13], flexomagnetolectric effects [14] or novel dynamic spin-wave properties [15,16] which can be exploited for high-dense spin-based solid-state information storage and processing combined in the same device. The skyrmion lattice is stabilized by Dzyaloshinskii–Moriya (DM) interaction [17–19] in some non-centrosymmetric magnetic materials. This limits the pool of prospective materials for the design of the skyrmion lattices; moreover the relativistic DM interaction is commonly weak so the magnetic skyrmion lattice can be stable within a narrow temperature-field region (see Table 1 from Ref. [20]) which additionally hinders their application. The search of the opportunities for the use of ordinary magnetic materials to create the skyrmion lattices will help to overcome these obstacles.

In principle well-known magnetic bubble domains (MBD) which can be stabilized in YIG by applying external magnetic field have the topology of the magnetic skyrmions [20,21]. Nevertheless the nonconductive nature of this material makes it unsuitable to exploit the unique transport effects connected with the magnetic skyrmions. Some recent works suggest new approaches to stabilization of the skyrmion lattices in the materials without the DM interaction by different types of nanopatterning. The first idea is to place Co particles on the surface of the CoPt film with perpendicular anisotropy. In this case the exchange interaction between the magnetic vortex within the Co particle and magnetization in the CoPt film stabilizes skyrmion-like magnetization distribution in the film below the magnetic vortices. This approach was corroborated by micromagnetic simulation [22] and even found the experimental verification [23,24]. Nevertheless to initialize the skyrmion lattice in the sample this method involves sophisticated manipulations with the external magnetic field while the skyrmion charge density achieved in the experiment (and demonstrated in simulation) is less than  $1 \mu\text{m}^{-2}$ . Another suggested method is based on the idea of the spatial modulation of the magnetic film thickness [25,26]. The micromagnetic simulations demonstrate the possibility of creation of dense enough (more than  $100 \mu\text{m}^{-2}$ ) skyrmion lattices in the nanopatterned magnetic films with perpendicular anisotropy, the skyrmions can be initialized by the simple magnetizing of the sample in the uniform external field. The idea is that by the varying the thickness of the film the domain wall will have the different energy in the different regions and this can prevent MBD (i.e. magnetic skyrmion) collapse or runoff.

In this paper we suggest the realization of the same idea by an

\* Correspondence address: Institute for Physics of Microstructures, RAS, Nizhny Novgorod 603950, GSP-105, Russia.

E-mail address: [msap@ipmras.ru](mailto:msap@ipmras.ru)

alternative method. Besides the spatial modulating of the film thickness it is possible to spatially modulate material parameters of the film to alter the domain wall energy. Indeed at the zero external field the MBD (topologically it is a magnetic skyrmion) have the tendency to runout. But if MBD is initially in the local region with the anisotropy value smaller than the anisotropy in the surrounding area the increase of the domain wall energy density (as  $\sigma_i = 4\sqrt{A_i K_i}$ ,  $K$  is anisotropy and  $A$  is exchange constant) will prevent the MBD runout outside the region with lesser anisotropy. Instead of the runout the MBD experienced squeeze if the thickness of the perpendicular magnetic films is less than some critical value [27]. In this case the local increase of the anisotropy value in the middle of the bubble domain can prevent its collapse due to the same mechanism. How is it possible to locally change the material parameters of the magnetic film? It is possible in the case of the superlattices of the alternating magnetic (Co and Fe) and nonmagnetic (Pt, Pd, Ru, Ir, Cu, and Au) layers that have perpendicular magnetic anisotropy [28]. Depending on the composition and the layer thicknesses the material parameters of the magnetic perpendicular medium are varied within the certain limits:  $M_s = 5 \times 10^5 - 18 \times 10^5$  A/m,  $K_u = 4 \times 10^5 - 4 \times 10^6$  J/m<sup>3</sup>, and  $A = 10^{-12} - 2 \times 10^{-11}$  J/m (it is the saturated magnetization, uniaxial anisotropy and exchange coefficient) [28–33]. In the case of the sufficiently thin magnetic layers the interlayer surface anisotropy is high enough to overcome the demagnetizing fields so the structure obtains the effective perpendicular easy axis anisotropy. The anisotropy coefficient depends on the interlayer surface roughness and so can be changed by He<sup>+</sup> [34,35] or Ga<sup>+</sup> [36] ions irradiation. Depending on the irradiation dose the value of the effective perpendicular anisotropy can be reduced or even becomes the easy-plane. The local change of the anisotropy coefficient can be achieved by use of the different masks with the holes of the necessary diameter or by the direct irradiation by the focused ion beams, the spatial resolution of such technique is up to 1 nm [37]. This is more than enough to form the periodic structures as represented in Fig. 1a, with the lattice period less than 100 nm and the irradiated areas as small as 50 nm in diameter. In the same way it is possible to reduce the anisotropy of the film leaving the anisotropy unchanged in the periodically arranged circular areas. In this case  $K_1 > K_0$ .

The aim of the presented work is to answer two questions: (1) Is it possible to stabilize the skyrmion (skyrmion lattice) by

such spatial modulation of the anisotropy value? (2) If “yes”, whether there is an easy way to initialize the skyrmion lattice in such periodically modulated film? The positive answers will open new ways to experimental realization of the skyrmion lattices in the ordinary magnetic materials at room temperature.

## 2. Analytical approach to the problem of the skyrmion stability in the area with changed material parameters

Here we consider the problem of the MBD stability in the infinite magnetic film which have the cylindrical area with the different material parameters as illustrated in Fig. 1a and b. The region 0 (periphery) represents the homogeneous material characterized by the parameters of magnetic anisotropy  $K_0$  and exchange energy  $A_0$  while the region 1 (circular central part) defined from  $r=0$  to  $r=r_0$  represents the area with changed values of the material parameters  $K_1$  and  $A_1$ . The easy direction of the anisotropy is everywhere perpendicular to the film. It is assumed that the saturation magnetization  $M_s$  is similar for the both regions. The film thickness is equal to  $h$ . Consider a cylindrical bubble of radius  $r$  where center coincides with the center of the coordinates. The total energy of the system is

$$W = W_\sigma + W_H + W_D \tag{1}$$

The first term  $W_\sigma$  is the domain wall energy of the MBD, the second term  $W_H$  is the interaction with the external magnetic field, the last one is the demagnetizing energy  $W_D$  of a single cylindrical domain in an infinite film. The problem is very similar to the well-known problem of the MBD stability in the homogeneous magnetic film, but one should take into account now that the domain wall energy per unit area depends on the domain wall position:  $\sigma_i = 4\sqrt{A_i K_i}$ , where  $A_i$  and  $K_i$  are the exchange and the anisotropy constants of the corresponding region. Besides let us take into account two facts: (1) in the real system the boundary between the regions with the different material parameters will be blurred and (2) the domain wall has its own thickness which is equal to  $2\pi\sqrt{A_i/K_i} \sim 5-10$  nm. So while domain wall shifts from the region 0 to region 1 it changes its energy fluently. In the frameworks of our model we use the following dependence of the domain wall energy density on its position:

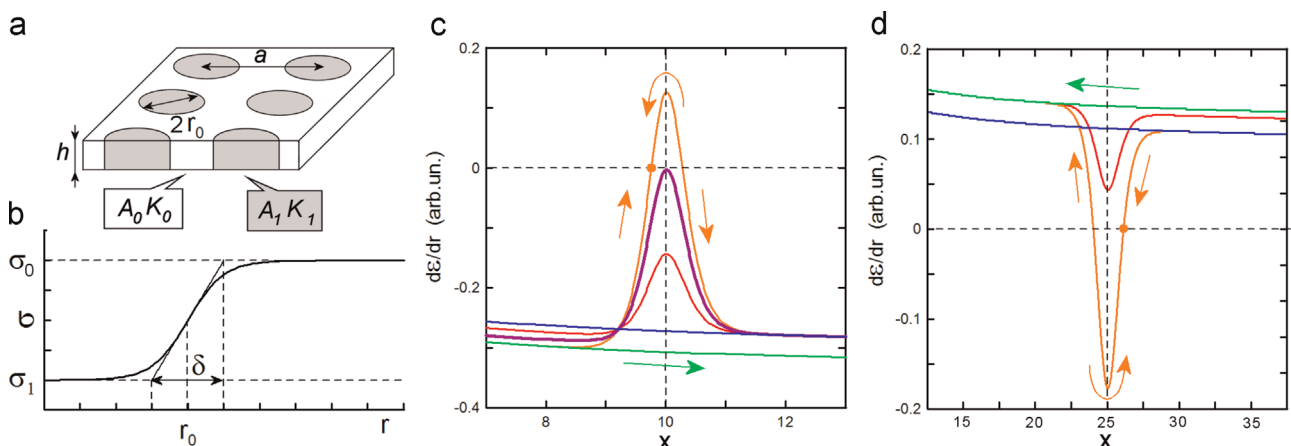


**Fig. 1.** (a) The geometry of suggested nanomodification:  $h$  is the film thickness,  $2r_0$  is the diameter of the area with modified material parameters, and  $a$  is the period. (b) The density of the domain wall energy profile in the system. (c) The  $x$  dependence of the  $dE/dr$  for the system with  $x_0 = 10$ ,  $\Delta = 0.85$  and  $\lambda_0 = 0.7$ . The upper line having peak (orange) is for  $\lambda_1 = 0.64$  (MBD is stable), the lower line having peak (red) is for  $\lambda_1 = 0.68$  (MBD is unstable). The thickest line (violet,  $\lambda_1 = 0.66$ ) corresponds to the boundary of the MBD stability. The monotonous lines (green and blue) are for the uniform magnetic film with  $\lambda_1 = \lambda_0 = 0.64$  and  $\lambda_1 = \lambda_0 = 0.7$  (MBD is unstable). (d) The  $x$  dependence of the  $dE/dr$  for the system with  $x_0 = 25$ ,  $\Delta = 1.84$  and  $\lambda_1 = 1.76$ . The lower line having valley (orange) is for  $\lambda_1 = 1.71$  (MBD is stable), the upper line having valley (red) is for  $\lambda_1 = 1.74$  (MBD is unstable). The monotonous lines (green and blue) are for the uniform magnetic film with  $\lambda_1 = \lambda_0$  (MBD is unstable). (For interpretation of the references to color in this figure caption, the reader is referred to the web version of this paper.)

$$\sigma(r) = \frac{\sigma_0 + \sigma_1}{2} + \frac{\sigma_0 - \sigma_1}{2} \tanh \frac{r - r_0}{\delta/2} \quad (2)$$

The phenomenological parameter  $\delta$  characterizes the spatial scale where the domain wall density changed its value. Evidently it cannot be less than the domain wall thickness. The equilibrium radius of the domain is to be determined by the conditions  $dE/dr = 0$ ,  $d^2E/dr^2 = 0$ . We will introduce the dimensionless energy, magnetic field, radius and characteristic length  $\lambda$  for simplicity:

$$\epsilon = W/16\pi^2 M_s^2 h^3, \quad (3)$$

$$\mathcal{H} = H/4\pi M_s, \quad (4)$$

$$x = r/h. \quad (5)$$

The dimensionless characteristic length depends on the dimensionless radius  $x$  as  $\sigma$  depends on  $r$ :

$$\lambda(x) = \frac{\sigma(x)}{4\pi h M_s^2} = \frac{\lambda_0 + \lambda_1}{2} + \frac{\lambda_0 - \lambda_1}{2} \tanh \frac{x - x_0}{\Delta/2}. \quad (6)$$

Here index  $i$  denotes corresponding region,  $x_0 = r_0/h$  and  $\Delta = \delta/h$ . So the dependence of the bubble domain energy on its radius takes the form of

$$\epsilon(x) = x\lambda(x)/2 + \mathcal{H}x^2 + \epsilon_D(x) \quad (7)$$

Now let us find the derivatives of each term in this expression on  $x$ . For the first term it is

$$\frac{d\epsilon_\sigma(x)}{dx} = \frac{\lambda_0 + \lambda_1}{4} + \frac{\lambda_0 - \lambda_1}{4} \tanh \frac{x - x_0}{\Delta/2} + \frac{2(\lambda_0 - \lambda_1)x}{\Delta(\exp(2(x - x_0)/\Delta) + \exp(2(x_0 - x)/\Delta))^2} \quad (8)$$

The derivative of the second term is evident. For the magnetostatic energy term we can use the known solution for the magnetostatic energy of the MBD in the uniform film as we assume saturation magnetization to be equal in both regions of the film. The necessary derivative of the magnetostatic energy of the MBD was obtained by Thiele [38,39] in the form of complete elliptic integral of the second kind. Instead of it we will use here the easy rational function

$$\frac{d\epsilon_D(x)}{dx} = -\frac{x}{1 + 3x/2} \quad (9)$$

suggested in [40] which demonstrates very good match with the exact Thiele's expression but much more suitable to obtain transparent final formulas. The calculated typical curves of  $d\epsilon/dx$  for the possible system parameters are represented in Fig. 1c and d for the zero external field. We do not derive the expression for  $d^2\epsilon/dx^2$ , nevertheless its sign can be easily determined from the plotted graphs for of  $d\epsilon/dx$ .

It is well known that an MBD is unstable at the zero external field in homogenous film. Depending on the film thickness and material parameters it expands or vice versa has a tendency to squeeze and collapses. The first situation is represented in Fig. 1c. The dimensionless values used for the curves calculation corresponds to the following dimensional geometrical  $h=10$  nm,  $r_0=100$  nm,  $\delta=8.5$  nm and material  $M_s = 9.5 \times 10^5$  A/m,  $A_1 = A_0 = 5 \times 10^{-12}$  J/m parameters. The different curves of  $d\epsilon/dx$  on the graph correspond to different anisotropy values. Two monotonous curves are plotted for uniform films with  $K_0 = 8 \times 10^5$  J/m<sup>3</sup> (upper, blue) and  $K_0 = 6.5 \times 10^5$  J/m<sup>3</sup> (lower, green).  $d\epsilon/dx < 0$  in these cases corresponds to runout instability of the MBD which is usual for the thick uniform films at zero

external field. In the case when the  $\lambda_1$  value (or anisotropy  $K_1$ , in the term of dimensional parameters) inside the central area decreases in comparison with the characteristic length or anisotropy of the rest of the film the situation changes – the local maximum appears on the  $d\epsilon/dx$  line. If this difference in the material parameters is not large the maximum do not reach the value of 0 and the MBD remains unstable (red line,  $K_0 = 8 \times 10^5$  J/m<sup>3</sup>,  $K_1 = 7.5 \times 10^5$  J/m<sup>3</sup>). But with the further decrease of the  $K_1$  value the maximum of the  $d\epsilon/dx$  grows up and finally reaches 0 (thick violet line  $K_0 = 8 \times 10^5$  J/m<sup>3</sup>,  $K_1 = 6.97 \times 10^5$  J/m<sup>3</sup>). At this moment the MDB becomes stable and stay stable with the further decrease of  $K_1$  in comparison with  $K_0$ . For example the orange line corresponded to  $K_0 = 6.5 \times 10^5$  J/m<sup>3</sup> cross the 0 value level twice. So the MBD can have two equilibrium radii  $x = x_{1,2}$  in this case,  $d\epsilon/dx = 0$  for the both points. Nevertheless it is evident from the graph that the less value  $x = x_1$  corresponds to the condition  $d^2\epsilon/dx^2 > 0$  as  $d\epsilon/dx$  grows up in this point. So this equilibrium radius of the MBD is stable. The large value  $x_2$  corresponds to the unstable MBD as  $d^2\epsilon/dx^2 < 0$  in this point. The arrows in Fig. 1c denote the duration of the MBD radius changing while it relaxes to the stable value. The external magnetic field directed against MBD magnetization gives the positive addition  $\mathcal{H}x$  to the  $d\epsilon/dx$  increasing the stability of the MBD; the same way the magnetic field directed along the MBD magnetization decreases its stability.

Fig. 1d demonstrates the dependencies of  $d\epsilon/dx$  on the MBD radius for the “thin” film when an MBD collapses in the homogenous film at the zero external field ( $d\epsilon/dx > 0$  for  $\lambda_1 = \lambda_0$ ). All the dimensional parameters are the same like in the previous case excluding film thickness  $h$  which is 4 nm instead of 10 nm. Nevertheless this leads to renormalization of all other dimensionless parameters like  $x_0$ ,  $\Delta$  and  $\lambda_i$  and qualitatively changed the behavior of the system. To avoid the MBD collapse it is necessary for  $\lambda_1$  (or correspondingly  $K_1$ ) to exceed  $\lambda_0$  (or correspondingly  $K_0$ ) in this case. If this difference is enough to decrease  $d\epsilon/dx$  below 0 at the boundary, the MBD becomes stable. Let us remember that the graphs are plotted for zero external field. Evidently the magnetic field acts in this case in the opposite way in comparison with the “thick” film case. The field directed along MBD magnetization improves the conditions for its stabilization, the magnetic field directed in the opposite direction decreases the MBD stability.

The condition

$$\max(d\epsilon/dx) = 0 \quad (10)$$

which is fulfilled for thick violet line in Fig. 1c determines the boundary of the MBD stability. Evidently  $d^2\epsilon/dx^2 = 0$  is the point where the first derivative has its maximum. The condition (10) links the geometrical and material parameters of the system and allow to obtain the MBD stability diagram. Due to the fact that  $d\epsilon_D(x)/dx + \mathcal{H}x$  are the slowly varying functions near  $x_0$  at the scale  $\Delta$  in comparison with  $d\epsilon_\sigma(x)/dx$  the position of  $d\epsilon/dx$  maximum practically coincides with  $x_0$ . This reason allows us to reduce the condition (10) to the  $d\epsilon/dx|_{x_0} = 0$  which has a form of

$$\left. \frac{d\epsilon}{dx} \right|_{x_0} = \frac{\lambda_0 + \lambda_1}{4} + \frac{\lambda_0 - \lambda_1}{2} \frac{x_0}{\Delta} + \mathcal{H}x_0 - \frac{x_0}{1 + 3x_0/2} = 0 \quad (11)$$

It is easy now to obtain expressions for the critical values of the material and geometrical parameters of the system which determines the stability boundaries of MBD, for example:

$$\lambda_{1c}(\lambda_0, x_0, \mathcal{H}) = \left( \frac{2x_0 + \Delta}{2x_0 - \Delta} \right) \lambda_0 + \frac{\mathcal{H}x_0 - x_0/(1 + 3x_0/2)}{x_0/2\Delta - 1/4} \quad (12)$$

or

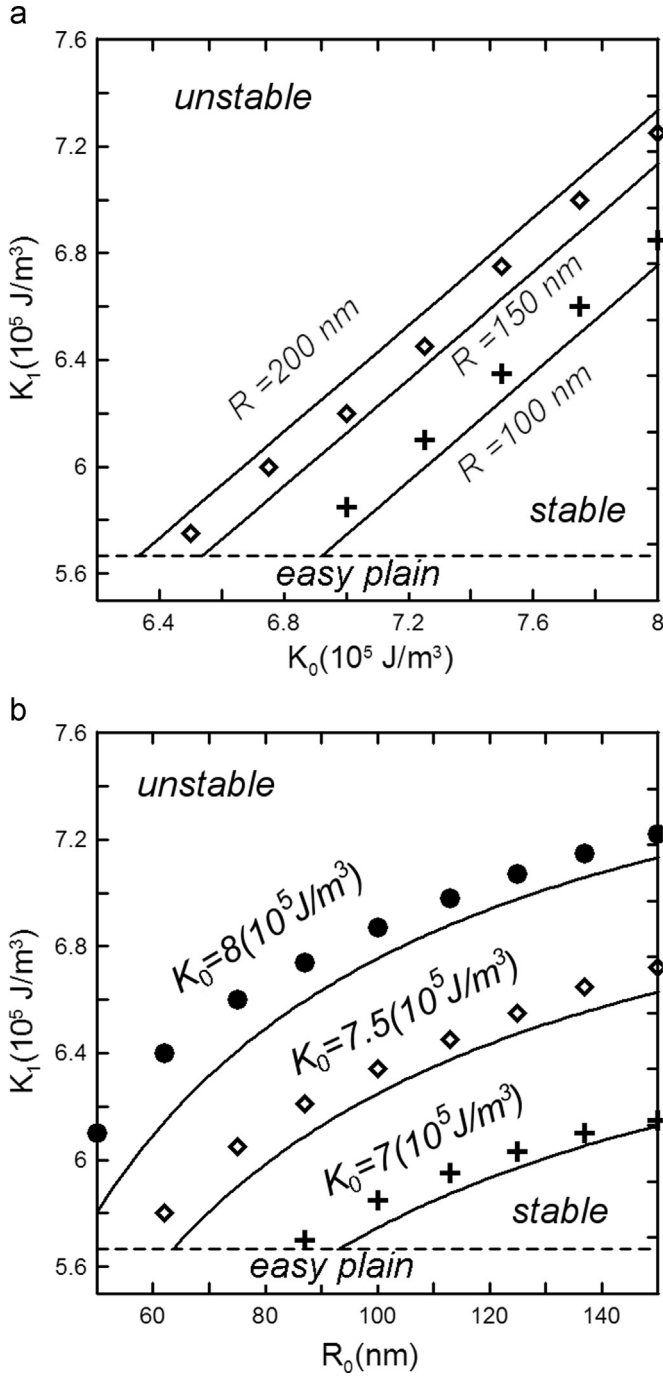


**Fig. 2.** The analytically calculated boundaries of the regions of the stable existence of the MBD at the zero external field plotted in different axes. The geometrical parameters of the system are the following:  $h = 10$  nm,  $\delta = 10$  nm,  $M_s = 9.5 \times 10^5$  A/m,  $A_1 = A_0 = 5 \times 10^{-12}$  J/m, and  $K_0 = 8 \times 10^5$  J/m<sup>3</sup> for the right graph. The dotted line denotes the value of  $K_1 = \mu_0 M_s^2 / 2$  which corresponded to effective easy plain anisotropy. The results of the micromagnetic simulations for the systems with the same material parameters are represented by symbols. The results of micromagnetic calculations for  $R_0 = 200$  nm are not present on the upper graph.

$$\mathcal{H}_c(\lambda_1, \lambda_0, x_0) = \frac{1}{1 + 3x_0/2} - \frac{\lambda_0 + \lambda_1}{4x_0} - \frac{\lambda_0 - \lambda_1}{2\Delta} \quad (13)$$

The stability diagrams plotted in the dimensional axes are represented in Fig. 2 for the case of the “thick” film. The same diagrams can be easily plotted for the case of the “thin” film using the same condition.

So our calculations demonstrate that it is possible to stabilize

MBD in the magnetic film which have the material parameters with the values usual for the ordinary magnetic materials with perpendicular magnetic anisotropy by appropriate spatial modulations of the perpendicular anisotropy value. The Dzyaloshinskii–Moriya interaction is not necessary in this case, the stabilization can be achieved at zero external field. The diameter of the stable MBD can be small enough (up to 50 nm) producing the corresponding high skyrmion charge density in the system.

### 3. Numerical simulations

So we analytically solve the problem of the skyrmion stability in the circular area with modified material parameters for the case when the anisotropy of the mentioned area is still easy axis. We corroborate our analytical approach with micromagnetic simulations utilizing the OOMMF code [41]. This code is based on a numerical solution of the system of Landau–Lifshitz–Gilbert (LLG) equations for the magnetization of the system. The geometry of the simulated system is the following: the rectangular plate with the circular area with the changed material parameters in the center. The width of the plate is within the limits 100–600 nm, its thickness is 5–15 nm, and the diameter of the central part is 50–300 nm. The grid size is  $2.5 \times 2.5 \times 2.5$  nm<sup>3</sup>. The periodical boundary conditions in the plane are applied to simulate the periodical lattice as presented in Fig. 1a. The material parameters of the system is chosen within the limits discussed in the introduction,  $K_1 < K_0$ .

We check the stability of the MBD placed in the central area with the reduced anisotropy value for different geometrical and material parameters. We carry out the simulations for the  $600 \times 600$  nm plate with the periodical boundary conditions at the zero external field. The boundaries for the values of the system parameters when the MBD remains stable and does not exhibit the expansion from the region with the reduced anisotropy are represented in Fig. 2. The good coincidence of the analytical calculations and the micromagnetic simulation is evident. The slight increase for the stability area for simulated system on the diagrams is likely caused by the following reason. Analytically we calculate the infinite film with the MBD alone. It is impossible to simulate exactly the same system. In the simulations the calculations are carried for the MBD placed in the center of the finite plate. In the second case the values of the demagnetizing fields causing the MBD instability are slightly less.

Besides the verification of the MBD stability the another interesting question is the possibility to initialize magnetic skyrmion in the initially uniformly magnetized system by applying the external magnetic field. At the first stage we simulated possible magnetic configurations arising in the system. Let us notice here that if the anisotropy coefficient is less than the critical value  $K_{1c} = \mu_0 M_s^2 / 2$  the effective anisotropy (taking into account the demagnetizing fields) becomes the “easy plain” type. In our micromagnetic simulations we studied both the system with  $K_1 > K_c$  and with  $K_1 < K_c$ . A starting point for the calculations is the uniformly magnetized film ( $M_z = -M_s$ ) and then the system relaxes in a stationary state. We add very small random anisotropy ( $K_r = 0.0001 \times K_0$ ) to introduce some inhomogeneity in the system and to initialize possible instability. The external magnetic field is equal to 0. Depending on the geometrical and material parameters the system stays stable in the uniformly magnetized state, relaxes to the labyrinth domain structure or forms one of the localized states represented in Fig. 3. There are the schematic pictures of the magnetization configuration as well as the distribution of the skyrmion charge density in the corresponding state defined as [8]

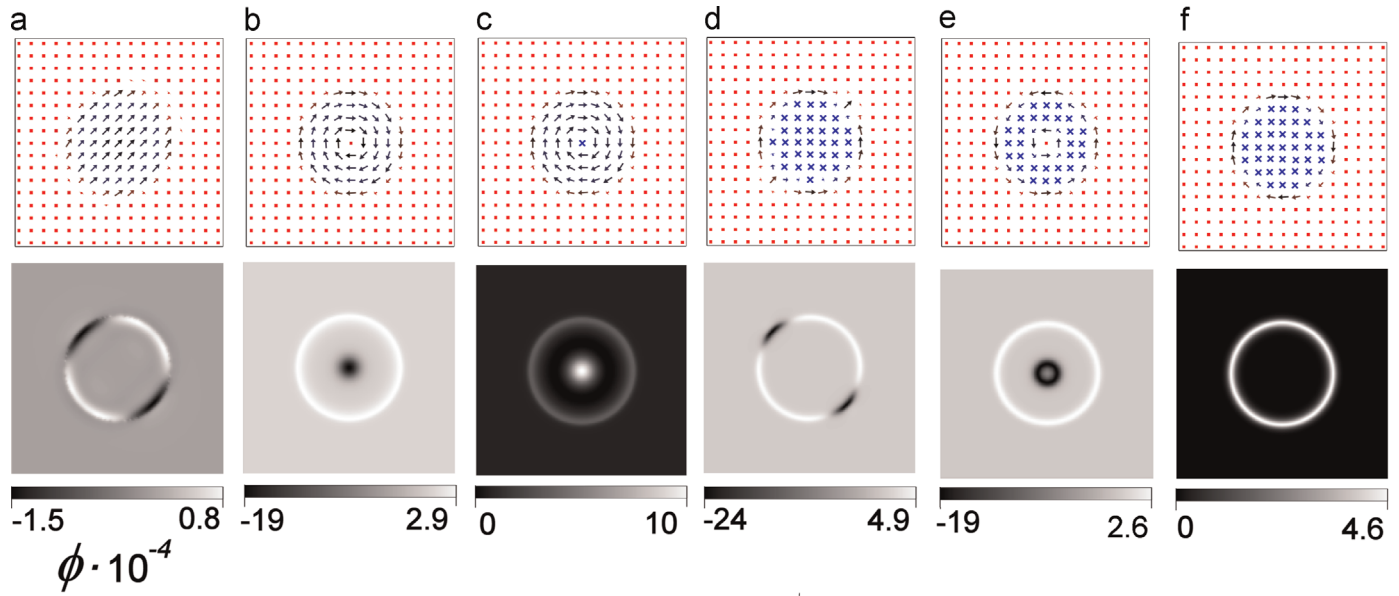


**Fig. 3.** The possible localized magnetization configurations existing in the magnetic film with the perpendicular anisotropy in the cylindrical area with the reduced anisotropy value: (a) SD – single domain, (b) CV – co-directional vortex, (c) OV – opposite magnetic vortex, (d) ON – onion, (e) CD – circular domain, and (f) MB – magnetic bubble. The top row is the scheme of the magnetization distribution in the film plane. Points (red) and crosses (blue) denote the magnetic moments directed perpendicular to the film plane in the opposite directions. The bottom row is the scheme of the topological charge density distribution for the corresponding states. The grid size is  $1 \times 1 \times 1 \text{ nm}^3$  for the calculations in this case. (For interpretation of the references to color in this figure caption, the reader is referred to the web version of this paper.)

$$\phi = \frac{1}{4\pi} \mathbf{n} \cdot \frac{\partial \mathbf{n}}{\partial x} \times \frac{\partial \mathbf{n}}{\partial y}, \quad (14)$$

$\mathbf{n} = \mathbf{M}(\mathbf{r})/|\mathbf{M}(\mathbf{r})|$  is the orientation of the magnetization. For the reference we named this states as “single domain” (SD – Fig. 3a), “co-directional vortex” (CV – Fig. 3b), “opposite magnetic vortex (OV – Fig. 3c), “onion” (ON – Fig. 3d), “circular domain” (CD – Fig. 3e) and “magnetic bubble” (MB – Fig. 3f). The first three states (SD, CV and OV) take place when the effective anisotropy of the central circular area is the easy plane, while the last three ones can be realized in the case when the anisotropy of the central circular area is still effectively easy axis.

All these states have the non-coplanar magnetization distribution, i.e. their local density of the skyrmion charge is not equal to zero. Nevertheless if one integrates the skyrmion charge density over the system the result will be different for different states.  $\int \phi(xy) dx dy = 0$  for SD, CV, ON and CD, so they do not carry topological charge. Vice versa OV and MB have the integral skyrmion charge equal to 1, so topologically they are the skyrmions. In

these two states the magnetization continuously changes from up direction in the center to down at the periphery in all radial directions away from the center and wraps a sphere pointing in all directions as it usual for skyrmion. In the case of the MB the skyrmion charge density is concentrated near domain wall, while in the case of the OV the topological charge is divided equally between the vortex core (1/2) and the wall between the vortex and the periphery (also 1/2). In the CV the topological charge carried by vortex core ( $-1/2$ ) is totally compensated by the topological charge carried by the wall between the vortex and periphery (1/2), so it can be continuously deformed to the uniform state.

The realization of the particular state after the relaxation from the uniformly magnetized state depends on the geometrical and material parameters of the system. Two examples of the possible “phase diagram” for the systems with different material parameters are represented in Fig. 4. They demonstrate that the topologically charged states can be distinguished by the simple demagnetizing from the uniformly saturated state for the wide range

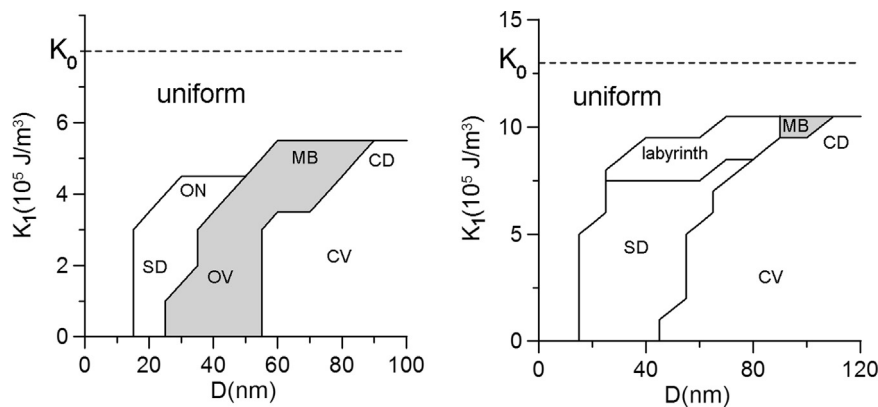


**Fig. 4.** The states appeared in the nanomodified film at the zero external field after relaxation from the saturated state (the result of the micromagnetic simulation). The geometrical parameters are the same for the left and right diagrams. System size is  $200 \times 200 \times 10 \text{ nm}^3$  with the periodical boundary conditions in the XY plane. Left: the material parameters of the film are  $M_s = 8.5 \times 10^5 \text{ A/m}$ ,  $K_0 = 8 \times 10^5 \text{ J/m}^3$ ,  $A = 5 \times 10^{-12} \text{ J/m}$ . Right:  $M_s = 1.35 \times 10^6 \text{ A/m}$ ,  $K_0 = 13 \times 10^5 \text{ J/m}^3$ ,  $A = 2 \times 10^{-11} \text{ J/m}$ . The axes represent the values of the diameter and anisotropy constant of the modified cylindrical area in the center of the simulated cell. The magnetic states correspond to the states in Fig. 3. Gray color denotes the states carrying the topological charge.

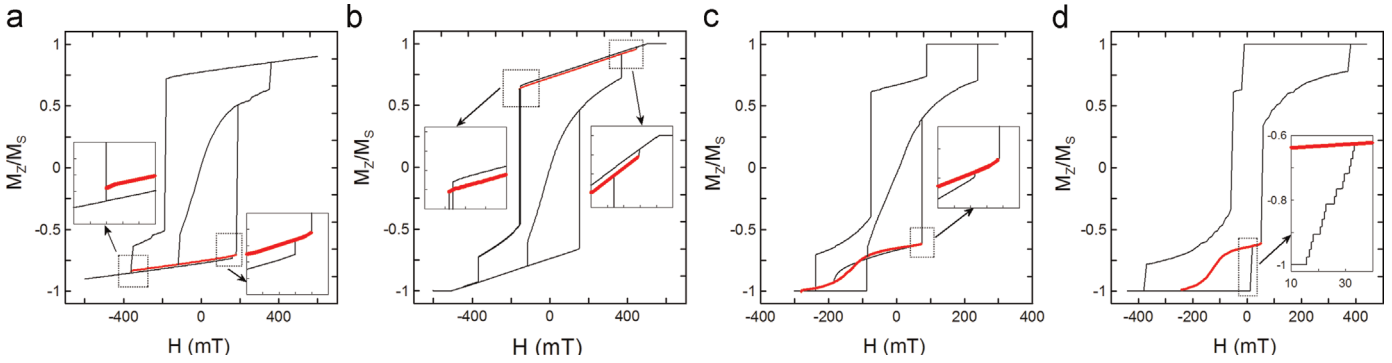


**Fig. 5.** The possible shapes of the hysteresis curves for the 200 nm × 200 nm piece of the 10 nm thick magnetic film ( $M_s = 9.5 \times 10^5$  A/m,  $A_1 = A_0 = 5 \times 10^{-12}$  J/m,  $K_0 = 8 \times 10^5$  J/m<sup>3</sup>) with the round 100 nm in diameter area with the modified value of anisotropy  $K_1$ . The periodical boundary conditions are applied to simulate the periodical lattice. (a)  $K_1 = 0$  J/m<sup>3</sup>, (b)  $K_1 = 3 \times 10^5$  J/m<sup>3</sup>, (c)  $K_1 = 5 \times 10^5$  J/m<sup>3</sup>, (d)  $K_1 = 5.5 \times 10^5$  J/m<sup>3</sup>. The thick red line is the branch of the hysteresis curve corresponding to the skyrmion formation. (For interpretation of the references to color in this figure caption, the reader is referred to the web version of this paper.)

of the initial material parameters of the magnetic film in the case of the proper nanomodification. The transformation of OV state to MB state takes place fluently with the increase of  $K_1$  and accompanied by a gradual expansion of the vortex core. The same gradual transitions are between SD and ON states as well as between CV and CD states. Therefore the boundaries between them are not denoted in Fig. 4. Arbitrarily the value  $K_{1c} = \mu_0 M_s^2 / 2$  which corresponds to the effective anisotropy change from the easy plain to the easy axes can be considered at such boundary.

The application of the uniform external magnetic film can cause transitions between the localized states. So it will allow to prepare the topologically charged states for wider ranges of the material and geometrical parameters of the system. For example Fig. 5 represents numerically calculated magnetization hysteresis curves for a 200 nm × 200 nm piece of the 10 nm thick magnetic film with periodical boundary condition. The following material parameters are used:  $M_s = 9.5 \times 10^5$  A/m,  $A_1 = A_0 = 5 \times 10^{-12}$  J/m, and  $K_0 = 8 \times 10^5$  J/m<sup>3</sup>. The cylindrical 100 nm diameter area with the modified value of anisotropy  $K_1$  is situated in the center of the cell. According to the results represented in Fig. 4 (left) in the case of the simple demagnetizing from the saturated state the formation of CV or CD states takes place for these values of the system parameters. These states do not carry topological charge but by applying uniform external field they can be transformed into the topologically charged OV and MB states which are the skyrmions. Depending on the  $K_1$  value four possible scenarios of the magnetizing process are possible. If  $0 \leq K_1 \leq 0.45 \times 10^5$  J/m<sup>3</sup> (Fig. 5a) at some critical field the reverse of the CV core magnetization takes place and it becomes OV state which still stays stable if the field is reduced to zero. Vice versa with the further increase of the external field OV become unstable and the labyrinth domain structure forms. In the case of  $0.45 \times 10^5$  J/m<sup>3</sup>  $\leq K_1 \leq 3.6 \times 10^5$  J/m<sup>3</sup> the increase of the magnetic field causes the developing of the labyrinth domain structure in the surrounding film before the reversal of the CV core in the central area takes place. The further increase of the magnetic field leads to the widening of the reversed domains, and finally the process ends with the total reversal of the film with the exception of the central area where the magnetic vortex still takes place. As its core is still unreversed and now it is directed against the film magnetization this state is topologically charged OV. It stays stable after reducing the field to zero, the increase of the field leads to the reversal of the OV core and the system again came to uncharged CV state. For  $4.4 \times 10^5$  J/m<sup>3</sup>  $\leq K_1 \leq 5.4 \times 10^5$  J/m<sup>3</sup> (Fig. 5c) the formation of the CD is observed with the following reversal of its core and transformation to the topologically charged MB state. The last scenario is observed for  $5.4 \times 10^5$  J/m<sup>3</sup>  $\leq K_1 \leq 5.6 \times 10^5$  J/m<sup>3</sup> (Fig. 5d). In this case the increase of the external field leads to the direct

conversion of the uniform state which is stable at  $H=0$  (see Fig. 4a also) to topologically charged MB state.

In most of our calculations we simulate the periodical lattice by one cell with the periodical boundary conditions. This method significantly increases the calculation rate but does not allow to resolve the magnetization structures which have the period larger than the period of nanomodification. The complex skyrmion lattices can appear due to the effective antiferromagnetic magneto-static interactions between the localized states [25]. This interaction is especially noticeable in the case of MB as their magnetic moment is significantly larger than the magnetic moment of the OV due to the larger volume of the core which is magnetized perpendicularly. To understand how does the inter-cell interaction influence the behavior of the system we carry out simulation of the 800 × 800 nm piece of the 10 nm thick magnetic film which contains 16 cylindrical areas arranged in the square lattice. The periodical boundary condition is also applied. The material parameters are the same as presented above. The general form of the hysteresis is the same as represented in Fig. 5d. The only evident difference is the appearance of the tiny devil-staircase structure (Fig. 5d, inset) on the magnetization curve branch corresponding to the process of the one-by-one MB appearing in the system. During this process the skyrmion lattices with different symmetries successively appear in the system until the dense skyrmion lattice is finally formed. All of them are stable at the zero magnetic field. The nature of the devil-staircase-like magnetization curves in systems with effective antiferromagnetic interaction even at nonzero temperatures is discussed in Refs. [25,42] in details.

#### 4. Conclusions

So we analytically solve the problem about the stability of the magnetic skyrmion in the thin magnetic film with the easy axis anisotropy in the absence of the DMI inside the area with the changed material parameters. This allows us to suggest the method for creating two-dimensional artificial lattice of magnetic skyrmions by spatial nanomodification of the easy-axis magnetic film. The calculations demonstrate that the appropriate material parameters of the initial magnetic film can be within the wide ranges which correspond to the known parameters of Co/Pt, Co/Pd, Co/Ru, Fe/Pd and the similar ferromagnetic/nonmagnetic superlattices. Wherein the achieved skyrmion charge density can be more than 100 per  $\mu\text{m}^2$ . The derived expressions allow one to easily estimate the parameters (geometrical and material) of the nanomodification which is necessary to obtain the stable skyrmion lattice in the real experiment. Besides by numerical micro-magnetic simulations we demonstrate that the skyrmion lattices

can be initialized in the system in the simple process of the magnetization in the uniform external field. It is well known that the coercivity of the perpendicular magnetic films can be significantly less than anisotropy. The magnetization reversal can start with appearance of the reversed nucleus in the “weak” place in this case. As for micromagnetic simulation this effect can be achieved by introducing some additional small random anisotropy. This random anisotropy can have larger value inside the modified area that is in good correspondence with the experimental data.

## Acknowledgments

This research is supported by the Russian Foundation for Basic Research (RFBR) (Grant no. 15-02-03046) and by Ministry of Education and Science of the Russian Federation (Agreement nos. 02.B.49.21.0003 and 14.578.21.0041, the Lobachevskii State University of Nizhny Novgorod).

## References

- [1] I.E. Dzyaloshinskii, B.A. Ivanov, JETP Lett. 29 (1979) 540.
- [2] A.S. Kovalev, A.M. Kosevich, K.V. Maslov, JETP Lett. 30 (1979) 296.
- [3] S. Muhlbauer, B. Binz, F. Jonietz, C. Pfleiderer, A. Rosch, A. Neubauer, R. Georgii, P. Boni, Science 323 (2009) 915.
- [4] X.Z. Yu, Y. Onose, N. Kanazawa, J.H. Park, J.H. Han, Y. Matsui, N. Nagaosa, Y. Tokura, Nature (London) 465 (2010) 901.
- [5] S. Heinze, K. von Bergmann, M. Menze, J. Brede, A. Kubetzka, R. Wiesendanger, G. Bihlmayer, S. Blugel, Nat. Phys. 7 (2011) 713.
- [6] U.K. Rossler, N. Bogdanov, C. Pfleiderer, Nature (London) 442 (2006) 797.
- [7] Y. Onose, N. Takeshita, C. Terakura, H. Takagi, Y. Tokura, Phys. Rev. B 72 (2005) 224431.
- [8] A. Neubauer, C. Pfleiderer, B. Binz, A. Rosch, R. Ritz, P.G. Niklowitz, P. Boni, Phys. Rev. Lett. 102 (2009) 186602.
- [9] B. Binza, A. Vishwanath, Physica B 403 (2008) 1336.
- [10] M. Lee, W. Kang, Y. Onose, Y. Tokura, N.P. Ong, Phys. Rev. Lett. 102 (2009) 186601.
- [11] F. Jonietz, S. Muhlbauer, C. Pfleiderer, A. Neubauer, W. Munzer, A. Bauer, T. Adams, R. Georgii, P. Boni, R.A. Duine, K. Everschor, M. Garst, A. Rosch, Science 330 (2010) 1648.
- [12] X.Z. Yu, N. Kanazawa, W.Z. Zhang, T. Nagai, T. Hara, K. Kimoto, Y. Matsui, Y. Onose, Y. Tokura, Nat. Commun. 3 (2012) 988.
- [13] J. Zang, M. Mostovoy, J.H. Han, N. Nagaosa, Phys. Rev. Lett. 107 (2011) 136804.
- [14] A.K. Zvezdin, A.P. Pyatakov, Phys.-Uspekhi 52 (2009) 845.
- [15] O. Petrova, O. Tchernyshyov, Phys. Rev. B 84 (2011) 214433.
- [16] M. Mochizuki, Phys. Rev. Lett. 108 (2012) 017601.
- [17] A. Bogdanov, A. Hubert, J. Magn. Magn. Mater. 138 (1994) 255.
- [18] A. Bogdanov, A. Hubert, J. Magn. Magn. Mater. 195 (1999) 182.
- [19] H.Y. Kwon, K.M. Bu, Y.Z. Wu, C. Won, J. Magn. Magn. Mater. 324 (2012) 2171.
- [20] N. Nagaosa, Y. Tokura, Nat. Nanotechnol. 8 (2013) 899.
- [21] B.A. Ivanov, V.A. Stepanovich, A.A. Zhmudskii, J. Magn. Magn. Mater. 88 (1990) 116.
- [22] L. Sun, R.X. Cao, B.F. Miao, Z. Feng, B. You, D. Wu, W. Zhang, An Hu, H.F. Ding, Phys. Rev. Lett. 110 (2013) 167201.
- [23] B.F. Miao, L. Sun, Y.W. Wu, X.D. Tao, X. Xiong, Y. Wen, R.X. Cao, P. Wang, D. Wu, Q.F. Zhan, B. You, J. Du, R.W. Li, H.F. Ding, Phys. Rev. B 90 (2014) 174411.
- [24] J. Li, A. Tan, K.W. Moon, A. Doran, M.A. Marcus, A.T. Young, E. Arenholz, S. Ma, R.F. Yang, C. Hwang, Z.Q. Qiu, Nat. Commun. 5 (2014) 4704.
- [25] M.V. Sapozhnikov, O.L. Ermolaeva, Phys. Rev. B 91 (2015) 024418.
- [26] A.I. Marchenko, V.N. Krivoruchko, J. Magn. Magn. Mater. 377 (2015) 153.
- [27] Equation (4.9) in T.H. O'Dell, Ferromagnetodynamics. The Dynamics of Magnetic Bubbles, Domains and Domain Walls The MacMillan Press Ltd., London, 1981.
- [28] M.T. Johnson, P.J.H. Bloemen, F.J.A. den Broeder, J.J. de Vries, Rep. Prog. Phys. 59 (1996) 1409.
- [29] C.J. Lin, G.L. Gorman, C.H. Lee, R.F.C. Farrow, E.E. Marinero, H.V. Do, H. Notarys, C.J. Chien, J. Magn. Magn. Mater. 93 (1991) 194.
- [30] K. Mizunuma, S. Ikeda, J.H. Park, H. Yamamoto, H. Gan, K. Miura, H. Hasegawa, J. Hayakawa, F. Matsukura, H. Ohno, Appl. Phys. Lett. 95 (2009) 232516.
- [31] C.L. Canedy, X.W. Li, Gang Xiao, Phys. Rev. B 62 (2000) 508.
- [32] M.T. Johnson, R. Jungblut, P.J. Kelly, F.J.A. den Broeder, J. Magn. Magn. Mater. 148 (1995) 118.
- [33] G.A. Bertero, R. Sinclair, J. Magn. Magn. Mater. 134 (1994) 173.
- [34] C. Chappert, H. Bernas, J. Ferre, V. Kottler, J.-P. Jamet, Y. Chen, E. Cambril, T. Devolder, F. Rousseaux, V. Mathet, H. Launois, Science 280 (1998) 1919.
- [35] T. Devolder, J. Ferre, C. Chappert, H. Bernas, J.-P. Jamet, V. Mathet, Phys. Rev. B 64 (2001) 064415.
- [36] A. Aziz, S.J. Bending, H. Roberts, S. Crampin, P.J. Heard, C.H. Marrows, J. Appl. Phys. 98 (2005) 124102.
- [37] Yu.I. Latyshev, A.P. Orlov, A.V. Frolov, V.A. Volkov, I.V. Zagorodnev, V. A. Skuratov, Yu.V. Petrov, O.F. Vyvenko, D.Yu. Ivanov, M. Konczykowski, P. Monceau, JETP Lett. 98 (2013) 214.
- [38] A.A. Thiele, Bell Syst. Tech. J. 48 (1969) 3287.
- [39] A.A. Thiele, J. Appl. Phys. 41 (1970) 1139.
- [40] H. Callen, R.M. Josephs, J. Appl. Phys. 42 (1971) 1977.
- [41] M.J. Donahue, D.G. Porter, OOMMF User's Guide Version 1.0, National Institute of Standards and Technology, Gaithersburg, MD, 1999.
- [42] A.A. Fraerman, M.V. Sapozhnikov, Phys. Rev. B 65 (2002) 184433.